Doping dependence of the phase diagram in one-dimensional extended Hubbard model: a functional renormalization group study

IOP Publishing Journal Title
Journal of Physics: Condensed Matter **XX** (XXXX) XXXXXX https://doi.org/XXXX/XXXX

Doping dependence of the phase diagram in one-dimensional extended Hubbard model: a functional renormalization group study

Yuan-Yuan Xiang[1], Xiao-Jie Liu[1,2], Ying-Han Yuan[1], Jie Cao[1], and Chun-Mei Tang[1]

[1] Department of Physics, College of Science, Hohai University, Nanjing, China
[2] Institute of Mechanics, Chinese Acadamy of Science, Beijing, China

E-mail: yyxiang@hhu.edu.cn

Received xxxxxx
Accepted for publication xxxxxx
Published xxxxxx

Abstract

Using functional renormalization group method, we studied the phase diagram of the one-dimensional extended Hubbard model at different dopings. At half filling, variety of states strongly compete with each other. These states include spin-density wave, charge-density wave, *s*-wave and *p*-wave superconductivity, phase separation, and an exotic bond-order wave. By doping, system favours superconductivity more than density waves. At 1/8 doping, a new area of extended *s*-wave superconductivity emerges between charge density wave and bond-order wave regions. If the system is doped to 1/4-doping, a new area of *p*-wave superconductivity emerges between charge-density wave and spin-density wave regions.

Keywords: functional renormalization group (FRG), extended Hubbard model (EHM), phase diagram (PD), bond-order wave (BOW), charge-density wave (CDW), spin-density wave (SDW), *s*-wave superconductivity (SSC), *p*-wave superconductivity (PSC)

1. Introduction

The one-dimensional extended Hubbard model (1d-EHM) is a practicable simple model for describing strong electronic correlations in quasi-one-dimensional (Q1D) materials. At half-filling, a important feature is the existence of the exotic bond-order wave(BOW) between spin-density wave(SDW) and charge-density wave(CDW)[1] and a tricritical point at intermediate coupling strength for repulsive interaction[2,3]. Superconductivity(SC) and phase separation(PS) will emerge for attractive interactions[4]. Until now, part or full of its half-filling phase diagram(PD) on the $U-V$ plane has been studied by exact diagonalization(ED)[4–6], g-ology[7–9], quantum Monte-Carlo(QMC)[2,3,5,10,11], density-matrix renormalization group[12–18], and some other theoretical methods[19–24]. In the scheme of functional renormalization group(FRG) which provides an unbiased approach to handle strongly-correlated systems with many possible competing instabilities, Tam *et al* get the BOW state at weak-coupling region[25]. However, the full PD at half-filling haven't been invested by FRG until now.

For real Q1D superconductors such as $K_2Cr_3As_3$ and related materials with the same structure[26–29], KCr_3As_3[30–32] and $K_2Mo_3As_3$[33], the system is doped away from half-filling. The pairing is proposed to be unconventional spin-triplet pairing induced by electron-electron correlations.[26,34] Despite of multi-band electronic structure of the real materials, study of the PD of doped one-band 1d-EHM may elucidate the effects of doping and correlation on possible electronic instabilities. Previously, *p*-wave spin-triplet pairing have only be found on $V<0$ region for 1d-EHM at both half-filling and quarter-doping, while no SC is found for repulsive interactions. Inspired by our previous FRG calculations, we may expect unconventional pairing induced by spin or charge fluctuations upon doping.

Motivated by the above two considerations, we ultilize the recently developed singular-mode FRG(SMFRG) method to

study the PD of 1d-EHM at different dopings. The paper is organized as follows. In Sec. 2, we introduce the model and method. In Sec. 3, we first give the phase diagram at half-filling as a benchmark of SMFRG method in one dimension. Then we give the PD at two specific dopings to show the effects of doping. In the last, we give some discussions and our conclusion.

2. Model and Methods

The model hamiltonian reads:

$$H = -t\sum_{i,\sigma}\left(c_{i,\sigma}^{\dagger}c_{i+1,\sigma} + h.c.\right) + U\sum_{i} n_{i,\uparrow}n_{i,\downarrow} + V\sum_{i} n_i n_{i+1}$$

where $c_{i,\sigma}$ is the annihilation operator of spin σ on site i, $n_i = \sum_\sigma n_{i,\sigma} = \sum_\sigma c_{i,\sigma}^{\dagger}c_{i,\sigma}$ is electron number operator on site i. t is the hopping integral on nearest neighbor(NN) bonds which is set to 1 during our calculation. We define the filling factor $f = n_e/2$ (n_e is the average number of electrons per-site) and the doping level $\delta = f - 1/2$. U and V are on-site and NN interactions respectively. During our calculation, we confined the interaction parameter space to be $U \in [-5,5]$, $V \in [-3,3]$ (in unit of t).

We utilize the SMFRG method to determine possible instabilities in this model. Details of FRG can be found in ref. [35] and here we give the basic ideas of SMFRG. The general four-point vertex function in the interaction $c_{k_1}^{\dagger}c_{k_2}^{\dagger}(-\Gamma_{1234})c_{k_3}c_{k_4}$ is rearranged into the pairing(P), crossing(C) and direct(D) channels in such a way that a collective momentum q can be associated and the other momentum dependence can be decomposed as:

$$\Gamma_{k+q,-k,-p,p+q} \to \sum_{mn} f_m^*(k)P_{mn}(q)f_n(p),$$
$$\Gamma_{k+q,p,k,p+q} \to \sum_{mn} f_m^*(k)C_{mn}(q)f_n(p),$$
$$\Gamma_{k+q,p,p+q,k} \to \sum_{mn} f_m^*(k)D_{mn}(q)f_n(p).$$

Here $\{f_m\}$ is a set of orthonormal lattice form factors, which describe the form of the fermion bilinears. Principally, the decomposition is rigorous if all form factors--the number of which diverges in the thermodynamic limit--is considered. Actually, only a finite set of form factors truncated up to a certain range are important in a potentially diverging scattering mode. For example, limiting the fermion bilinears to site-local spin-density and d-wave pairing on 1st NN bonds proved already successful for the Hubbard model describing cuprates.[36] In this paper, we choose the following seven form factors:

$$f_0(k) = 1;$$
$$f_1^s(k) = \sqrt{2}\cos k\,;\ f_1^p(k) = \sqrt{2}\sin k\,;$$
$$f_2^s(k) = \sqrt{2}\cos 2k\,;\ f_2^p(k) = \sqrt{2}\sin 2k\,;$$
$$f_3^s(k) = \sqrt{2}\cos 3k\,;\ f_3^p(k) = \sqrt{2}\sin 3k\,;$$

where the subscripts 1,2,3 denote 1st NN, 2nd NN, 3rd NN respectively. We have checked that longer-range form factors will not affect the results qualitatively.

We considered all one-loop correction to the vertex function and the partial flow equations for each channel can be written as:

$$\frac{\partial P}{\partial \Lambda} = P\chi'_{pp}P,$$
$$\frac{\partial C}{\partial \Lambda} = C\chi'_{ph}C,$$
$$\frac{\partial D}{\partial \Lambda} = (C-D)\chi'_{ph}D + D\chi'_{ph}(C-D),$$

where Λ is the flowing energy scale (the infrared limit of the Matsubara frequency in our case) and $\chi'_{pp/ph}$ are loop integrations projected by the form factors:

$$\left(\chi'_{pp}\right)_{mn} = -\frac{1}{2\pi}\int\frac{dk}{2\pi}f_m(k)G(k+q,i\Lambda)G(-k,-i\Lambda)f_n^*(k) + (\Lambda\to-\Lambda),$$
$$\left(\chi'_{ph}\right)_{mn} = -\frac{1}{2\pi}\int\frac{dk}{2\pi}f_m(k)G(k+q,i\Lambda)G(k,i\Lambda)f_n^*(k) + (\Lambda\to-\Lambda),$$

where G is the bare fermion propagator. As usual FRG implementation, the self-energy correction and frequency dependence of the vertex function are ignored. The full flow equations can be written as:

$$\frac{dP}{d\Lambda} = \frac{\partial P}{\partial \Lambda} + \hat{P}\left(\frac{\partial C}{\partial \Lambda} + \frac{\partial D}{\partial \Lambda}\right)$$
$$\frac{dC}{d\Lambda} = \frac{\partial C}{\partial \Lambda} + \hat{C}\left(\frac{\partial P}{\partial \Lambda} + \frac{\partial D}{\partial \Lambda}\right)$$
$$\frac{dD}{d\Lambda} = \frac{\partial D}{\partial \Lambda} + \hat{D}\left(\frac{\partial P}{\partial \Lambda} + \frac{\partial C}{\partial \Lambda}\right)$$

where $\hat{P}, \hat{C}, \hat{D}$ are the projection operators which project the contributions from the other two channels.

It can be shown that the effective interaction in SC, SDW, and CDW channels are given by $V_{SC} = -P, V_{SDW} = C, V_{CDW} = C - 2D$ respectively. By singular-value decomposition, we monitor the evolution of the collective momentum q_X and the most-negative singular value S_X in channel X (X=SC, SDW, CDW). The flow is stopped if any of $|P|_{max}$, $|C|_{max}$, or $|D|_{max}$ becomes roughly ten times of the bandwidth or Λ is less than the mesh-gap due to discretization of the k points. The most diverging S_X at some critical scale Λ_c determines the leading instability. Form-factor of the order parameter is determined by the corresponding eigenvector of the decomposed effective interaction. In our calculation, CDW, PS and BOW instabilities are all in the CDW channel, with their differences

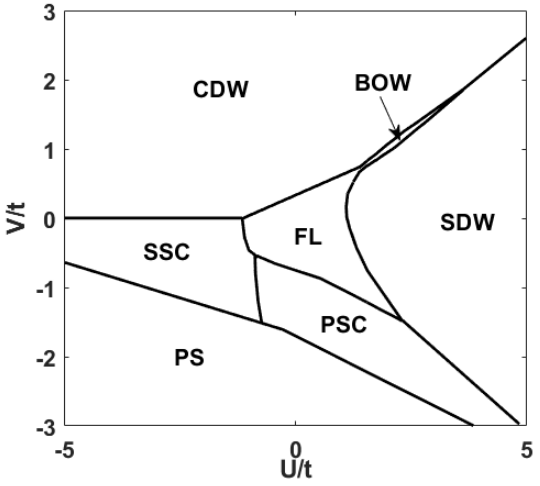

Figure 1. Phase diagram at half-filling. In the Fermi liquid(FL) region, no instability is found during our calculation.

lying in the collective momentums or form-factors which will be explained later.

3. Results

3.1 Phase diagram at half-filling

3.1.1 Three general phases and their boundaries

Fig. 1 shows our PHD of 1d-EHM at half filling which is consistent with previous DMRG results. The PHD can be roughly divided into three regions where the main instabilities are SDW, CDW, and PS respectively. The collective momentum for the three phases are π, π and 0 respectively. In the Fermi-liquid(FL) region, no divergence is found.

3.1.2 BOW phase

Around these three PB's, new states emerge as the leading instabilities. In the first quadrant, a narrow region of BOW phase emerges around the PB between SDW and CDW phases. As interaction strength increases, this region expands first and then shrinks into a tri-critical point around $(U, V) \sim (3.6, 1.8)$. Hence, we get all the main features naturally without any presumed assumptions. In this region, the SDW and CDW channel strongly compete with each other at high energy level. During the flow to lower energy level, CDW channel becomes logarithmically diverging after a crossover from on-site CDW state to extended p-wave CDW state, i.e. the BOW phase. From the final form factor and the associated wave vector $q_{BOW} = \pi$, we obtain the order parameter operator of the BOW phase in real space as:

$$\hat{O}_{BOW}(i) = (-1)^i \sum_{\sigma} \left(c^{\dagger}_{i,\sigma} c_{i+1,\sigma} + c^{\dagger}_{i+1,\sigma} c_{i,\sigma} \right)$$

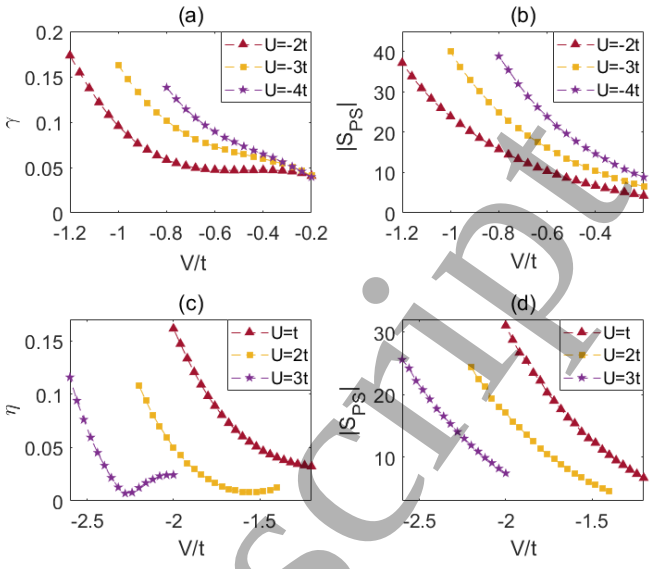

Figure 2. (a) Dependence of γ of SSC gap function on V for $U = -2$ (red triangle), $U = -3$ (yellow square), and $U = -4$ (purple pentagram) respectively. (b) The same as (a) but for the singular value of PS interaction vertex S_{PS} at the end of FRG flow. (c) Dependence of η of PSC gap function on V for $U = 1$ (red triangle), $U = 2$ (yellow square), and $U = 3$ (purple pentagram) respectively. (d)The same as (c) but for the singular value of PS interaction vertex S_{PS} at the end of FRG flow.

The sign factor $(-1)^i$ reveals the p-wave nature of this phase which renormalizing the effective hopping staggered along the 1d chain, leading to dimerization.

3.1.3 SC phases

Between CDW and PS, s-wave SC(SSC) becomes the leading instability. We found $U < 0$ for the whole SSC region. The pairing formfactor takes a general form $\alpha + \gamma \cos 2k$. In the majority of this area, the γ component is negligible, indicating the dominating intrinsic on-site pairing induced by attractive U. However, when close to the PS phases, the γ component becomes non-negligible. We plot the dependence of γ on V for there different U in Fig. 2(a). The range of V for a special U corresponds to a cut line of the SSC region. As we can see, the value of γ increases rapidly as V close to the lower boundary. We found that the dependence of S_{PS} in the

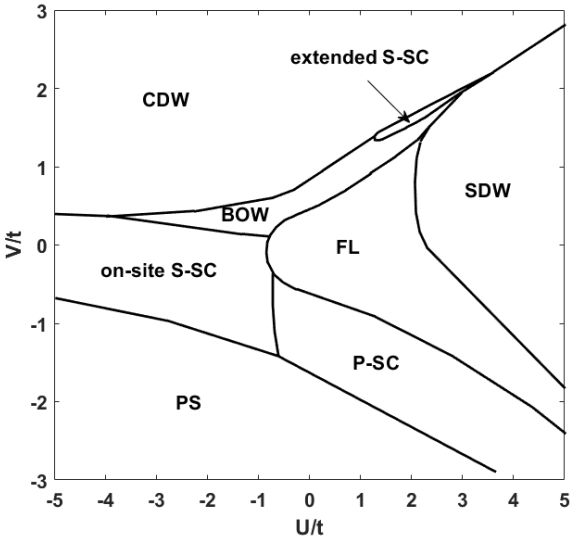

Figure 3. Phase diagram at 1/8 doping.

final step of FRG on V almost shows the same behaviour as shown in Fig. 2(b). By this comparison we conjecture that the γ component in SSC gap function is induced by the PS fluctuation.

Between SDW and PS, p-wave SC(PSC) becomes the leading instability. The gap form is written as $\beta \sin k + \eta \sin 3k$ for the whole region. We found that the η term is negligible in the majority of this region, indicating p-wave pairing is mainly on NN bonds which is induced directly by attractive V. This state is expected to have some similar aspects to that of the Kitaev chain model in which there appears Majorana edge states at the ends of the chain. [37] When close to PS region, the η term which corresponding to p-wave pairing on 3rd NN bonds becomes non-negligible. We plot the dependence of η and S_{PS} on V for three vertical cut lines with $U = 1,2,3$ in Fig.s 2(c) and (d). The similar behavior of η and S_{PS} indicate a positive correlation between them. Associating with the SSC cases we claim that the PS fluctuation may induce pairings on bonds.

As we can see, $f_1^s(k)$, $f_3^s(k)$ and $f_2^p(k)$ is missing in our SSC and PSC gap functions. At half-filling, they are energetically unfavorable since all of them generate nodes on the two Fermi points located at $\pm\pi/2$. We will see this is also true for the doping cases.

3.2 Results at 1/8 doping

The phase diagram at 1/8 doping is shown in Fig. 3 to see the effects of slight doping. The main features of the phase diagram are similar to that of half-filling. We will talk about the properties of the various phases in the following.

3.2.1 CDW, SDW and PS

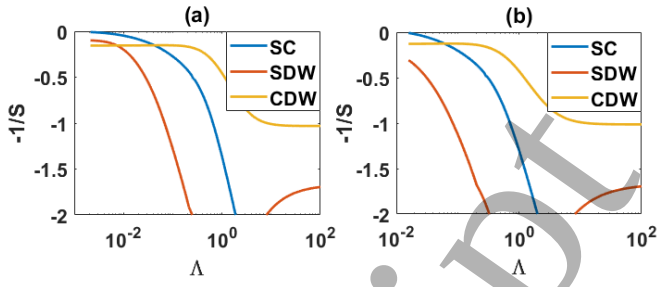

Figure 4. Flow diagrams for $U = 2.95, V = 1.95$ (a) and $U = 2.95, V = 1.97$ (b). The vertical axis is multiplied by 5 to enhance the visualization.

At 1/8-doping, we found the q-vector for SDW changes to 0.75π which is the nesting vector at this doping level. However, we found q_{CDW} remains to be π for the majority of the CDW region. On one hand, the bare effective interaction for CDW is $U + 2V\cos q$, which is most attractive at $q = \pi$. On the other hand, we found that the CDW channel diverges at high energy level in most cases, hence it can't take advantage of the nesting. If we going to the boundary of the CDW region, we found its critical scale decreases and its q-vector gradually evolves to q_{nest}. Properties of the PS state remains the same as half-filling case.

3.2.2 BOW

For BOW region, the form factor now can be written as $\alpha + \beta_1 \cos k + \gamma_1 \cos 2k + \beta_2 \sin k + \gamma_2 \sin 2k$. The first three terms correspond to on-site, NN, NNN s-wave particle-hole pairings and the latter two are NN and NNN p-wave particle-hole pairings. We found the main term two be α and β_2 for the whole region, indicating this phase can be simply regarded as a mixed state of CDW and BOW.(We refer to this phase as BOW for simplicity.) At first glance, the mixture of s- and p-wave seems conflict with the original C_{2v} lattice symmetry since the form-factor is not a irreducible representation of it. However, the wave vector associating with BOW now is $q_{BOW} = 0.75\pi$, which breaks the original lattice symmetry. In this sense, we conclude that the mixture of s- and p-wave phases is reasonable.

3.2.3 SC

At 1/8 doping, previous SSC and PSC regions slightly expand. The main pairing terms remain the same as the half filling case. However, since k_F changes to $3\pi/8$ now, $\cos k$ and $\sin 2k$ terms appear to be the minor pairings for SSC and PSC respectively. Surprisingly, we found a new narrow SC region between CDW and SDW phases in the first quadrant. In particle-hole channel, CDW and SDW fluctuation are comparatively strong in this region. For example, Figs. 4 shows the flow diagrams for $U = 2.95, V = 1.95$ in (a) and

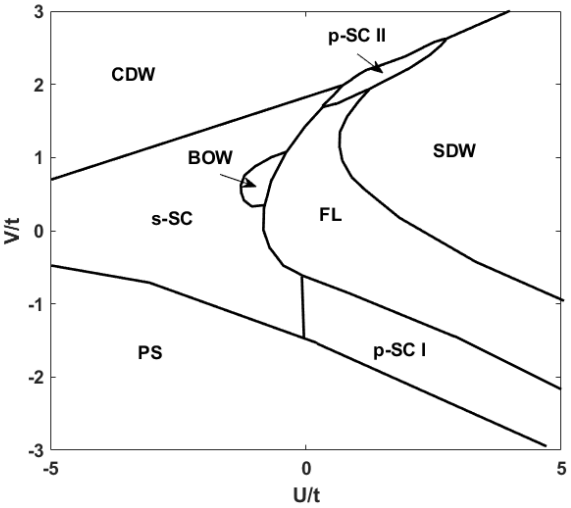

Figure 5. Phase diagram at 1/4 doping.

$U = 2.95, V = 1.97$ in (b). In the CDW channel, the leading q-vector is always located at π. Hence it cann't take advantage of the low-energy scatterings and saturates at high energy scale. However, in the SDW channel, the leading q-vector evolves form π to $2k_F = 0.75\pi$. Hence it still grows at low energy scale. The relative strength between CDW and SDW fluctuation depends on the final diverging energy scale as in the two cases we shown. The pairing function takes the form $\alpha + \beta \cos k + \gamma \cos 2k$ with β-term dominant, indicating a extended SSC state. From the real space configuration of the CDW and SDW fluctuations, we conjecture that they may both contribute to the extended SSC.

3.3 Results at 1/4 doping

Fig. 5 shows the PD of 1/4-doping. Properties of CDW, SDW and PS phases are similar to those of 1/8-doping. (Note that k_F changes to $\pi/4$ now.) The BOW region shrinks to a small region around the origin in the 2nd quadrant. The wave vector changes to $\pi/2$ and the form-factor can be written as $\alpha + \beta(\cos k + \sin k) + \gamma \sin 2k$ with α and β terms dominating. In the following, we focus on the properties of SC phases.

3.3.1 SSC

At 1/4-doping, previous SSC region significantly extends to $V > 0$ region. The main pairing remains on-site while the minor pairing changes with location on the $U - V$ plane. As we found, the minor pairing terms are $\cos k$ for $V < 0$ and $\cos 2k$ for $V > 0$. Both of their weights in the gap function increase with $|V|$. At the top right corner of this region $V \gg U > 0$, we found the weight of $\cos 2k$ term becomes

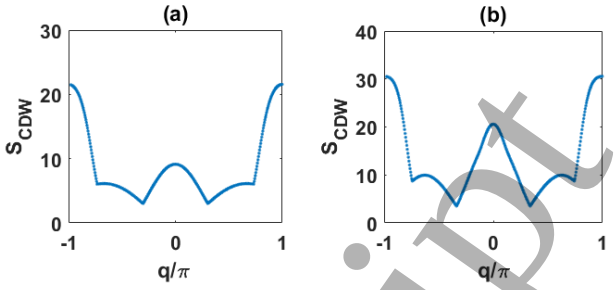

Figure 6. q-dependence of $S_{CDW}(q)$ for $U = 1.2, V = 1.99$ (a) and $U = 1.2, V = 2.14$ (b).

comparable to on-site term which is similar to the extended SSC case at 1/8 doping.

3.3.2 PSC

For PSC, there are two distinct regions on the PD. In PSC I region, the main pairing term is $\sin k$ which is pretty similar to the former two cases. In the PSC II region between SDW and CDW, no intrinsic pairing interaction exist since both U and V are repulsive. The gap function can be written as $\beta \sin k + \gamma \sin 2k$ with $\beta \approx \gamma$. The pairing mechanism is a little bit subtle. In this region, we found it's the $q = \pi$ CDW fluctuation or $q = \pi/2$ SDW fluctuation to be the dominating fluctuation in particle-hole channel. However, these two kinds of fluctuations both favor extended SSC with strongest pairing on NNN bonds, corresponding to $\cos 2k$ term in the gap function. At 1/4-doping, this pairing term is 0 at the two Fermi points, making it energetically unfavorable. So we further checked the subleading fluctuations in the particle-hole channel. As shown in Figs. 6, we found a second peak at $q = 0$ for $S_{CDW}(q)$. This corresponds to PS fluctuation which can induce the PSC obtained in our calculations.

4. Discussion and Conclusion

Here we compare some of our results with existing studies. At half-filling, we get a "FL" region which is absent in previous studies by ED, QMC, and DMRG. [6,10,11,14,15] This is due to our truncation of the flow parameter and interaction vertex since numerical calculations will become unreliable if we go further. At the truncation point, if we assume leading channel as the possible instability, the existing PD at half-filling can be recovered.

After doping, we found the q_{CDW} remains to be π, indicating a phase-separated state with high and low density regions. This is qualitatively consistent with ED and QMC calculations. [38,39] An important issue here is the existing of narrow SC regions found in the first quadrant on the $U - V$ plane, which seems to conflict with previous QMC study, in which the authors ruled out the possibility of SC for repulsive interactions.[39] They argue that although K_ρ has the

tendency to exceed one when approaching the boundary of PS, due to strong spin fluctuation SDW should be the leading instability. However, from FRG point of view, strong charge or spin fluctuations may induce unconventional SC such as the case of iron-based superconductors. The extended SSC for 1/8-doping here is consistent with this picture. For the PSC we found at quarter-filling, pairing is induced by $q = 0$ charge fluctuations. In this sense, we conclude our finding of SC for repulsive interactions is reasonable and we expect further confirmation by other methods.

It should be noted that our results should be understood by the competitions among different kinds of instabilities. Some non-perturbative features of one-dimensional correlated systems may not be properly captured by our FRG scheme. For example, Lieb and Wu found the ground state is Luttinger liquid for $U > 0, V = 0, \delta \neq 0$ via Bethe's ansatz.[40] Since the framework of FRG is based on Fermi liquids, it's hard to obtain Luttinger liquid or featureless Mott insulator without any long-range order. Whether inclusions of frequency dependence and higher order flow diagrams can overcome this difficulty is still an open question.

In summary, we studied the PD's of 1d-EHM at half-filling, 1/8-doping and 1/4-doping. The PD at half-filling showed the reliability of our SMFRG method in one dimension and intermediate coupling strength. Two doping PD's showed the possibility of new unconventional SC induced by charge or spin fluctuations in the particle-hole channel in this model. For the real Q1D superconductors, experimental results suggest possible spin-triplet pairing. Despite their multi-band electronic structure, our theoretical results based on one-band model may provide the possibility of triplet pairing induced by charge or spin fluctuations in Q1D systems.

Acknowledgements

We thank Qiang-Hua Wang and Da Wang from Nanjing University for helpful discussions. The work was Supported by National Science Foundation of China (under grant No. 11504085), Natural Science Foundation of Jiangsu Province (under grant No. BK20160854) and the Fundamental Research Funds for the Central Universities (under grant No. 2018B58714).

References

[1] Nakamura M 1999 Mechanism of CDW-SDW Transition in One Dimension *J. Phys. Soc. Japan* **68** 3123

[2] Hirsch J E 1984 Charge-Density-Wave to Spin-Density-Wave Transition in the Extended Hubbard Model *Phys. Rev. Lett.* **53** 2327

[3] Cannon J W and Fradkin E 1990 Phase diagram of the extended Hubbard model in one spatial dimension *Phys. Rev. B* **41** 9435

[4] Kuroki K, Kusakabe K and Aoki H 1994 Phase diagram of the extended attractive Hubbard model in one dimension *Phys. Rev. B* **50** 575

[5] Lin H Q, Campbell D K and Clay R T 2000 *Broken Symmetries in the One-Dimensional Extended Hubbard Model* vol 38

[6] Nakamura M 2000 Tricritical behavior in the extended Hubbard chains *Phys. Rev. B* **61** 16377

[7] Tsuchiizu M and Furusaki A 2002 Phase Diagram of the One-Dimensional Extended Hubbard Model at Half Filling *Phys. Rev. Lett.* **88** 056402

[8] Tsuchiizu M and Furusaki A 2004 Ground-state phase diagram of the one-dimensional half-filled extended Hubbard model *Phys. Rev. B* **69** 035103

[9] Ménard M and Bourbonnais C 2011 Renormalization group analysis of the one-dimensional extended Hubbard model *Phys. Rev. B* **83** 075111

[10] Sengupta P, Sandvik A W and Campbell D K 2002 Bond-order-wave phase and quantum phase transitions in the one-dimensional extended Hubbard model *Phys. Rev. B* **65** 155113

[11] Sandvik A W, Balents L and Campbell D K 2004 Ground State Phases of the Half-Filled One-Dimensional Extended Hubbard Model *Phys. Rev. Lett.* **92** 236401

[12] Zhang G P 1997 Ground-state phase diagram of the one-dimensional extended Hubbard model: A density-matrix renormalization-group approach *Phys. Rev. B* **56** 9189

[13] Jeckelmann E 2002 Ground-State Phase Diagram of a Half-Filled One-Dimensional Extended Hubbard Model *Phys. Rev. Lett.* **89** 236401

[14] Zhang Y Z 2004 Dimerization in a Half-Filled One-Dimensional Extended Hubbard Model *Phys. Rev. Lett.* **92** 246404

[15] Glocke S, Klümper A and Sirker J 2007 Half-filled one-dimensional extended Hubbard model: Phase diagram and thermodynamics *Phys. Rev. B* **76** 155121

[16] Ejima S and Nishimoto S 2007 Phase Diagram of the One-Dimensional Half-Filled Extended Hubbard Model *Phys. Rev. Lett.* **99** 216403

[17] Liu G-H and Wang C-H 2011 Existence of Bond-Order-Wave Phase in One-Dimensional Extended Hubbard Model *Commun. Theor. Phys.* **55** 702

[18] Li Y-C and Yuan Z-G 2016 Direct evidence of the BOW and TS states in the half-filled one-dimensional extended Hubbard model *Phys. Lett. A* **380** 272–6

[19] van Dongen P G J 1994 Extended Hubbard model at strong coupling *Phys. Rev. B* **49** 7904

[20] van Dongen P G J 1995 Phase Separation in the Extended Hubbard Model at Weak Coupling *Phys. Rev. Lett.* **74** 182

[21] Gu S-J, Deng S-S, Li Y-Q and Lin H-Q 2004 Entanglement and Quantum Phase Transition in the Extended Hubbard Model *Phys. Rev. Lett.* **93** 086402

[22] Bourbonnais C and Jérome D 2008 Interacting Electrons in Quasi-One-Dimensional Organic Superconductors *BOOK* pp 357–412

[23] Kumar M, Ramasesha S and Soos Z G 2009 Tuning the bond-order wave phase in the half-filled extended Hubbard model *Phys. Rev. B* **79** 035102

[24] Kumar M and Soos Z G 2010 Bond-order wave phase of the extended Hubbard model: Electronic solitons, paramagnetism, and coupling to Peierls and Holstein phonons *Phys. Rev. B* **82** 155144

[25] Tam K-M, Tsai S-W and Campbell D K 2006 Functional Renormalization Group Analysis of the Half-Filled One-Dimensional Extended Hubbard Model *Phys. Rev. Lett.* **96** 036408

[26] Bao J-K, Liu J-Y, Ma C-W, Meng Z-H, Tang Z-T, Sun Y-L, Zhai H-F, Jiang H, Bai H, Feng C-M, Xu Z-A and Cao G-H 2015 Superconductivity in Quasi-One-Dimensional K2Cr3As3 with Significant Electron Correlations *Phys. Rev. X* **5** 011013

[27] Zhang W-L, Li H, Xia D, Liu H W, Shi Y-G, Luo J L, Hu J, Richard P and Ding H 2015 Observation of a Raman-active phonon with Fano line shape in the quasi-one-dimensional superconductor K2Cr3As3 *Phys. Rev. B* **92** 060502

[28] Tang Z, Bao J, Wang Z, Bai H, Jiang H, Liu Y, Zhai H, Feng C-M, Xu Z-A and Cao G-H 2015 Superconductivity in quasi-one-dimensional Cs2Cr3As3 with large interchain distance *Sci. China Mater.* **58** 16–20

[29] Mu Q-G, Ruan B-B, Pan B-J, Liu T, Yu J, Zhao K, Chen G-F and Ren Z-A 2018 Ion-exchange synthesis and superconductivity at 8.6 K of Na2Cr3As3 with quasi-one-dimensional crystal structure *Phys. Rev. Mater.* **2** 034803

[30] Tang Z-T, Bao J-K, Liu Y, Bai H, Jiang H, Zhai H-F, Feng C-M, Xu Z-A and Cao G-H 2015 Synthesis, crystal structure and physical properties of quasi-one-dimensional ACr3As3(A = Rb, Cs) *Sci. China Mater.* **58** 543

[31] Mu Q-G, Ruan B-B, Pan B-J, Liu T, Yu J, Zhao K, Chen G-F and Ren Z-A 2017 Superconductivity at 5 K in quasi-one-dimensional Cr-based KCr3As3 single crystals *Phys. Rev. B* **96** 140504

[32] Liu T, Mu Q-G, Pan B-J, Yu J, Ruan B-B, Zhao K, Chen G-F and Ren Z-A 2017 Superconductivity at 7.3 K in the 133-type Cr-based RbCr3As3 single crystals *Europhys. Lett.* **120** 27006

[33] Mu Q-G, Ruan B-B, Zhao K, Pan B-J, Liu T, Shan L, Chen G-F and Ren Z-A 2018 Superconductivity at 10.4 K in a novel quasi-one-dimensional ternary molybdenum pnictide K2Mo3As3 *Sci. Bull.* **63** 952

[34] Wu X, Yang F, Le C, Fan H and Hu J 2015 Triplet pz-wave pairing in quasi one dimensional A2Cr3As3 superconductors *Phys. Rev. B* **92** 104511

[35] Metzner W, Salmhofer M, Honerkamp C, Meden V and Kurt S 2012 Functional renormalization group approach to correlated fermion systems *Rev. Mod. Phys.* **84** 299

[36] Husemann C and Salmhofer M 2009 Efficient parametrization of the vertex function, Ω scheme, and the t, t' Hubbard model at van Hove filling *Phys. Rev. B - Condens. Matter Mater. Phys.* **79** 195125

[37] Kitaev A 2000 Unpaired Majorana fermions in quantum wires *Physics-Uspekhi* **44** 131

[38] Mila F and Zotos X 1993 Phase Diagram of the One-Dimensional Extended Hubbard Model at Quarter-Filling *Eur. Lett.* **24** 133

[39] Clay R T, Sandvik A W and Campbell D K 1999 Possible exotic phases in the one-dimensional extended Hubbard model *Phys. Rev. B* **59** 4665

[40] Lieb E H and Wu F Y 1968 Absence of Mott Transition in an Exact Solution of the Short-

Range, One-Band Model in One Dimension
Phys. Rev. Lett. **20** 1445